Anticancer and Antimicrobial Screening of Novel Pyrazolo[2,3-*c*]pyridopyridazine Analogues: Synthesis, Spectral Characterization, Molecular Docking and Dynamics Studies

GAUTAM BHARDWAJ[1,] , SURESH KUMAR[2,*,] and RAJIV KUMAR TONK[1,*,]

[1]Department of Pharmaceutical Chemistry, School of Pharmaceutical Sciences, Delhi Pharmaceutical Sciences and Research University, Pushp Vihar, Sector-3, New Delhi-110017, India
[2]Division of Medical Laboratory Technology, School of Allied Health Science, Delhi Pharmaceutical Sciences and Research University, Pushp Vihar, Sector-3, New Delhi-110017, India

*Corresponding authors: E-mail: s.kumar@dpsru.edu.in; tonkrk@dpsru.edu.in

A major threat in cancer management is the development of drug resistance and gene mutations. Serine threonine kinases like DYRK1A pathway are potential targets for cancer therapies. In this work, a new series of seven pyrazolo[2,3-*c*]pyridopyridazine analogs were synthesized and characterized by spectroscopic methods. Three compounds were evaluated for *in-vitro* anticancer activity following 60 cell lines protocol of NCI, USA and for antimicrobial activity against Gram-negative and Gram-positive bacteria. All the compounds exhibited moderate to good antibacterial activity, while compounds **4a**, **4b** and **4d** showed moderate responses against leukemia, ovarian cancer, and prostate cancer cell lines in anti-proliferative studies.

Keywords: Pyrazolo[2,3-*c*]pyridopyridazine, DYRK1A inhibitors, Anticancer activity, Computational design.

INTRODUCTION

Cancer is one of the largest cause of mortality worldwide, contributing to over 10 million deaths in 2020 or roughly one in every six deaths (WHO). There are several treatments for cancers which may vary depending on the types and stages, as well as individual patient factors. Some common treatments for cancers are surgery, radiation therapy, chemotherapy, immunotherapy, targeted therapy, hormone therapy, stem cell transplant, precision medicine, *etc*. Moreover, bacterial infection also promotes progression and spread of cancer [1]. Despite all these treatment options, cancers still remain the main cause of death across the globe.

Kinases are a family of proteins in eukaryotes that regulate cellular function and processes. The serine threonine kinase family includes DYRK1A, which is involved in the development of cancer. Litovchick *et al*. [2] reported that DYRK1A participates in mTOR signaling pathway. Cancer chemotherapy, a common cancer treatment, involves killing both cancerous cells and normal cells. Since 1942, a major problem in cancer treat-ment has been the development of drug resistance and

the high cost of therapy [3]. DYRK1A is activated by self-phosphorylation, which is responsible for carcinogenesis and metastasis. Signal transducer and activator of transcription (STAT) proteins transmit signals from cell surface receptors to the nucleus in normal cells and at the same time, promote and progress cancer. STAT inhibit apoptosis and initiate angiogenesis and metastasis, observed in brain, solid tumors, hematological malignancies and prostate cancer [4].

DYRK1A is involved in the GLI1 sonic hedgehog pathway [5] as well as in Caspase-9 pathway [6-8]. Evidently, knockdown of DYRK1A consequently, leads to DNA damage-induced apoptosis [9]. Furthermore, DYRK1A is indirectly or directly involved in cancer drug resistance [10]. Thus, DYRK1A inhibitors synergize response in both chemo and radiotherapy in various tumors [11]. Natural DYRK1A inhibitors (Fig. 1) have a heterocyclic nucleus with its effective dose [12]. For example, harmine (**I**) (IC$_{50}$ = 80 nM) and harmol (**II**) (IC$_{50}$ = 90 nM) both have carbazole nucleus, whereas staurosporine (**III**) (IC$_{50}$ = 19 nM) has three fused indoles.

Acrifoline (**IV**), a quinolinone fused with benzopyran, and pyridazine (**V**), pyridine fused with pyridazine scaffolds,
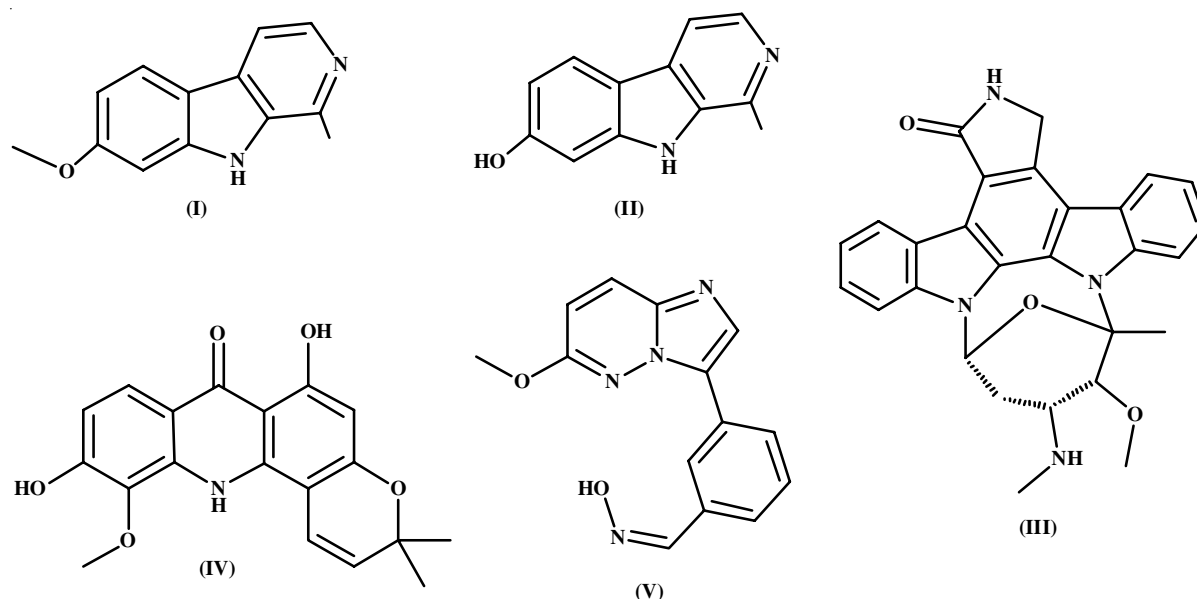
Fig. 1. Chemical structure of known DYRK1A inhibitor

have been found to be effective as anticancer, antidiabetic, analgesic, anti-inflammatory and anti-hypertensive agents [13]. However, there is a lack of structural similarity among the known DYRK1A inhibitors derived from natural products, except for the common feature of a fused heterocyclic system with three to four fused rings highlights the need for our current study. Thus, in this work a novel fused substituted pyrazolo-[4,3-*c*]pyrido[3,2-*e*]pyridazine compounds that have the potential to act as DYRK1A inhibitors were synthesized and characterized, thereby providing a new avenue for cancer treatment.

EXPERIMENTAL

All the reactions were carried out under laboratory conditions and the laboratory-grade reagents procured from CDH, LOBA, S.D. Fine, and Merck were utilized. The melting points of the compounds were determined using a digital melting point apparatus and are reported as uncorrected values. The spectral characterization was performed using a Bruker FT-IR and a 300 MHz ^{1}H NMR (Bruker DPX) spectrometer with DMSO-d_6 as solvent. The reaction progress was monitored using TLC plates.

Synthesis of pyrazolo[2,3-*c*]pyridopyridazine

Synthesis of ethyl-(2Z)-3-oxo-2-[2-(pyridin-2-yl)hydra-zinylidene]butanoate (2): A solution of 2-aminopyridine in a 1:1 mixture of water and conc. HCl was cooled to 0-5 ºC. While maintaining the temperature at 0-5 ºC, a saturated solution of sodium nitrite (0.13 mM) was added portion-wise with vigorous stirring to the cooled solution to form the diazonium salt. The prepared diazonium salt was added to a cooled mixture of ethyl acetoacetate (0.07 mM) and sodium acetate in ethanol (10.5 mL) and was then continuously stirred on a magnetic stirrer for 10 h. The resulting pale yellow mixture was extracted with chloroform and the solvent was evaporated to obtain a solid mass. Yield: 41%; m.p.: 150-152 ºC, R_f = 0.47. FT-IR

(KBr, ν_{max}, cm^{-1}): 3450, 1730, 1680, 1390. ^{1}H NMR (300 MHz, CDCl$_3$) δ ppm: 1.25 (t, 3H, CH$_3$, *J* = 6.5 Hz), 2.06 (s, 3H, COCH$_3$), 3.94 (q, 2H, OCH$_2$, *J* = 2.1 Hz), 6.15-7.44 (m, 4H, Ar-H), 8.14 (s, 1H, NH-D$_2$O exchangable). Anal. calcd. (found) % for C$_{11}$H$_{13}$N$_3$O$_3$: C, 56.16 (56.25); H, 5.57 (5.62): N, 17.86 (17.82).

Synthesis of *m*-acetylpyrido[2,3-*c*]pyridazin-4(1*H*)-one (3): A mixture of anhydrous AlCl$_3$ (37 mM) in chlorobenzene (30 mL) was added to compound (**2**) (13 mM) and the reaction mixture was stirred at room temperature for 1 h. Subsequently, the reaction mixture was heated at 120 ºC for 14-16 h. Upon completion of the reaction, it was worked up by adding 10% HCl and then basified using NaOH base to obtain 3-acetyl-pyrido[2,3-*c*]pyridazin-4(1*H*)-one (**3**) as precipitate. The obtained product **3** was washed with a benzene and ethanol mixture (1:1). The air dried product was rewashed and recrystallized with an acetic acid and methanol mixture (4:6) and then obtained as white solid. Yield: 3.8 g (47.5%); m.p.: 265-268 ºC, R_f = 0.92. FT-IR (KBr, ν_{max}, cm^{-1}): 3418, 1720, 1652. ^{1}H NMR (300Mz, DMSO-d_6): δ ppm: 1.88 (s, 3H, CH$_3$), 7.04 (s, 1H, NH, D$_2$O), 7.16-7.37 (m, 3H). Anal. calcd. (found) % for C$_9$H$_7$N$_3$O$_2$: C, 56.60 (56.55); H, 4.75 (4.79); N, 19.80 (19.88).

General synthesis of pyridopyridazine derivatives (4a-g): An equimolar quantity of the substituted aromatic acid hydrazide and 3-acetylpyrido[2,3-*c*]pyridazin-4(1*H*)-one (**3**) in a mixture of (0.29 mM) anhydrous 1,4-dioxane with 2-3 drops of conc. HCl was added. The reaction mixture was refluxed for 4-8 h and after completion of the reaction, the contents of the flask were reduced to one-third and left for 24 h at room temperature [14]. A solid product separated, which was filtered, washed and dried to obtain products (**4a-g**) (**Scheme-I**). The final product was recrystallized using ethyl acetate as solvent.

(3-Methyl-1*H*-pyrazolo[4,3-*c*]pyrido[3,2-*e*]pyridazin-1-yl)(phenyl)methanone (4a): White solid; yield: 60%; m.p.: 193-195 ºC; R_f = 0.6. FT-IR (KBr, ν_{max}, cm^{-1}): 1637, 1272, 841. ^{1}H NMR (300MHz, DMSO-d_6) δ ppm: 1.78 (s, 3H, CH$_3$), 7.18-8.27(m, 7H, Ar-H), 9.76 (s, 1H, Ar-H). HRMS (TOF-MS)
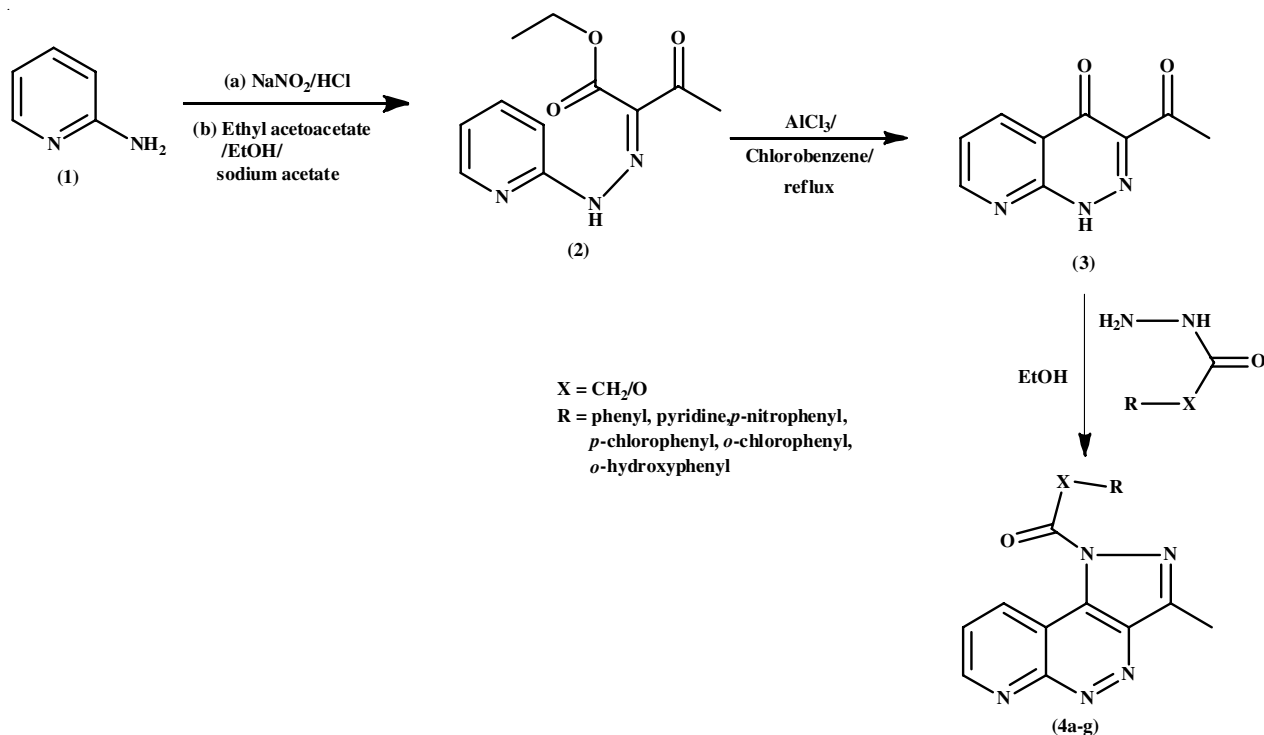
Scheme-I: Synthesis of new pyrido pyridazine compounds

(M+H)$^+$ m/z 289.1088. Anal. calcd. (found) % for C$_{16}$H$_{11}$N$_5$O: C, 66.43 (66.48); H, 3.38 (3.43); N, 24.21 (24.26).

(3-Methyl-1H-pyrazolo[4,3-c]pyrido[3,2-e]pyridazin-1-yl)(pyridin-3-yl)methanone (4b): Cream solid; yield: 70%; m.p.: 209-214 ℃; R$_f$ = 0.46. FT-IR (KBr, ν$_{max}$, cm^{-1}): 1733. ^{1}H NMR (300 MHz, DMSO-d_6) δ ppm: 1.87 (s, 3H, CH$_3$), 7.50-8.76 (m, 5H, ArH), 9.06 (s, 2H, Ar-H). HRMS (TOF-MS) (M+H)$^+$ m/z 291.0891. Anal. calcd. (found) % for C$_{15}$H$_{10}$N$_6$O: C, 62.06 (62.12); H, 3.47 (3.31); N, 28.95 (28.90).

1-(3-Methyl-1H-pyrazolo[4,3-c]pyrido[3,2-e]pyridazin-1-yl)-2-phenylethan-1-one (4c): Yellowish solid; yield: 63% ; m.p.: 182-185 ℃; R$_f$ = 0.47. FT-IR (KBr, ν$_{max}$, cm^{-1}): 1733, 1652. ^{1}H NMR (300 MHz, DMSO-d_6) δ ppm: 2.94 (s, 3H, CH$_3$), 4.04 (s, 2H, Ar-CH$_2$), 6.73-7.27 (m, 7H, Ar-H), 10.08 (s, 1H, Ar-H). Anal. calcd. (found) % for C$_{17}$H$_{13}$N$_5$O: C, 67.32; (67.28); H, 4.32 (4.37); N, 23.09 (23.01).

(3-Methyl-1H-pyrazolo[4,3-c]pyrido[3,2-e]pyridazin-1-yl)(4-nitrophenyl)methanone(4d): Yellow solid; yield: 62%; m.p.: 190-192 ℃; R$_f$ = 0.48. FT-IR (KBr, ν$_{max}$, cm^{-1}): 1733, 1473. ^{1}H NMR (300 MHz, DMSO-d_6) δ ppm: 1.93 (s, 3H, CH$_3$), 6.53-8.38 (m, 6H, Ar-H), 8.95 (s, 1H, Ar-H). HRMS (TOF-MS) (M+H)$^+$ m/z 334.0802. Anal. calcd. (found) % for C$_{16}$H$_{10}$N$_6$O$_3$: C, 56.94 (56.89); H, 4.07 (4.01); N, 22.13 (22.19).

(2-Chlorophenyl)(3-methyl-1H-pyrazolo[4,3-c]pyrido[3,2-e]pyridazin-1-yl)methanone (4e): Red solid, yield: 70%; m.p.: 186-188 ℃; R$_f$ = 0.47. FT-IR (KBr, ν$_{max}$, cm^{-1}): 1636, 1471. ^{1}H NMR (300 MHz, DMSO-d_6) δ ppm: 1.99 (s, 3H, CH$_3$), 6.48-6.62 (m, 3H, Ar-H), 7.13-7.51 (m, 3H, Ar-H), 9.70-10.22 (m, 1H, Ar-H). Anal. calcd. (found) % for C$_{16}$H$_{10}$N$_5$OCl: C, 59.36 (59.30); H, 3.11 (3.05); N, 21.63 (21.58).

(4-Chlorophenyl)(3-methyl-1H-pyrazolo[4,3-c]pyrido[3,2-e]pyridazin-1-yl)methanone (4f): Red solid, yield: 64%;

m.p.: 197-198 ℃; R$_f$ = 0.42. FT-IR (KBr, ν$_{max}$, cm^{-1}): 1637, 1570, 1473. ^{1}H NMR (300 MHz, DMSO-d_6) δ ppm: 1.92 (s, 3H, CH$_3$), 7.51-7.96 (m, 6H, Ar-H), 9.93-10.64 (m, 1H). Anal calcd. (found) % for C$_{16}$H$_{10}$N$_5$OCl: C, 59.36 (59.29); H, 3.11 (3.04); N, 21.63 (21.70).

(2-Hydroxyphenyl)(3-methyl-1H-pyrazolo[4,3-c]pyrido[3,2-e]pyridazin-1-yl)methanone (4g): Cream solid, yield: 43%; m.p.: 229-232 ℃; R$_f$ = 0.8. FT-IR (KBr, ν$_{max}$, cm^{-1}): 3309, 1616, 1348. ^{1}H NMR (300 MHz, DMSO-d_6) δ ppm: 1.92 (s, 3H, CH$_3$), 4.2 (s, 1H), 8.04-8.40 (m, 7H, Ar-H). Anal calcd. (found) % for C$_{16}$H$_{11}$N$_5$O$_2$: C, 62.95 (62.89); H, 3.63 (3.60); N, 22.94 (22.86).

For computational drug design, we used Structure-Based Drug Design (SBDD), Molecular Dynamics (MD) Simulation, and Molecular Mechanics Poisson-Boltzmann Surface Area (MMPBSA) techniques, utilizing open-source software. The protein structure retrieved from the RCSB database.

Software and Tools: All experimental *in silico* work was conducted using an Intel i-5 and Xeon processor with 16 GB of RAM. Protein preparation, structure drawing, and conversion to the working format were performed using open-source software, including Discovery Studio, ChemDraw and Open-Babel. The design of compound pharmacokinetics was determined using Swiss ADME. Docking and simulation experiments were performed using AutoDock Vina and GROMACS.

Pre-design pharmacokinetic parameters to determine drug likeness: ADME analysis was performed using Lipinski's Rule of Five, as determined by IT [15]. The bioavailability Radar tool in Swiss ADME was used to analyze physico-chemical properties and filter potent compound molecules. The bioavailability radar provides better results by evaluating six parameters, including solubility, size, polarity, lipophilicity, flexibility and saturation.

Protein selection, preparation and docking by using autodock vina: The structure based drug design was performed using the docking method, Autodock Vina [16,17] and visualization was done using Discovery Studio Visualizer [18]. The protein selected for SBDD DYRK1A inhibitor was obtained from the UniProt database with ID 13627 (PDB ID: 6Q8K) [19]. The 3D crystal structure of the protein (PDB ID: 6Q8K) was retrieved from the RCSB PDB website. The downloaded protein (PDB ID: 6Q8K) was prepared using Discovery Studio Visualizer, which involved the removal of hetero atoms and water, and MGL tools to add hydrogen and assignment of charges. Autodock Vina, only grid parameters were defined and then docking was performed. The docking results were further analyzed using Discovery Studio Visualizer.

Molecular Dynamic and MMPBSA: Molecular dynamics (MD) simulation was performed to further examine the stability of the complex after docking. The MD simulation was conducted using the GROMACS open source software with the CHARMM36 force field. The topology of the protein was prepared using the CHARMM36 force field and the ligand topology after processing was generated using the CGenFF server [20]. The two topology were then combined to create the complex topology. The next step involved immersing the complex in a dodecahedral cubic box filled with water. The solvated system was neutralized with three sodium counter ions. To equilibrate the system, NVT and NPT, and MD production runs were performed for 10 ns at 300 K and pressure of 1 bar. The simulation results were analyzed using RMSD, RMSF, radius of gyration, hydrogen bonding, van der Waals energy and electrostatic energy.

Binding free energy: The binding free energy was reanalyzed using the MMPBSA method [21] with the AMBER force field to determine the binding affinity. In MMPBSA, only AMBER force field applicable only.

Biological evaluation: The antimicrobial screening were performed by using nutrient agar media followed by cup plate method. The Gram positive *S. aureus* (ATCC 25923) and Gram negative *E. coli* (ATCC 25922) strains were used. The cell suspension of nutrient agar in plates where plugs were detached by sterile cork. The control where use solvent, test in DMSO and standard in triplicate to be placed in BOD for 24 h. The observation as zone of inhibition in millimeters to be recorded.

***in-vitro* Anticancer evaluation:** The anticancer activity of three compounds were screened against the 60 cell lines to be evaluated at N.C.I, USA.

RESULTS AND DISCUSSION

Synthesis of novel pyrazolo[2,3-*c*]pyridopyridazines (**4a-g**) was achieved from pyridine-2-amine (**1**) by diazotization reaction and followed by addition ethylacetoacetate with sodium acetate. The key intermediate (**2**) on further cyclization by using anhydrous AlCl₃ in chlorobenzene yield another key intermediate (**3**) containing pyridopyridazine nucleus. This heterocyclic system has a 1,3-dicarbonyl framework which upon addition of aryl hydrazine or aroyl hydrazines results in the regioselective synthesis of the final compounds **4a-g**. The structure of the synthesized compounds **2**, **3** and **4a-g** were succesfully elucidated. In intermediate **2**, the IR peak at 3450 cm⁻¹ (N-H), 1730 cm⁻¹ and 1680 (C=O) cm⁻¹ indicates the N-H stretching and carbonyl group. In NMR, the triplet and quatret of ester, singlet of a methyl group, multiplet of methyl group pyridopyridazine core. Intermediate **3** confirmed by the characteristic singlet of N-H shift to upshield at δ 7.0 ppm and similarly, the IR peak at 1720 and 1652 cm⁻¹ (C=O) confirmed the presence of diketonic groups. Intermediate **3** serves as diketone and subsequent condensation with acid hydrazides results in the formation of compounds **4a-g**. The disappearance of singlet of N-H at δ 7.0 ppm of intermediate **3** and upfield of methyl at δ 1.7 ppm in ¹H NMR confirmed the pyrazole ring formation.

In cancer drug discovery, designing to save time and money thus the significance of computational methods not deny and initiate the work. Toxicity and ADME (absorption, distribution, metabolism, and excretion) properties are the major drawbacks after finding a lead compound from hit compounds. In computational design, compounds **4a**, **4b** and **4d** were found to be non-violated.

ADME Analysis and theoretical target prediction: The ADME analysis on the designed compounds are listed in Table-1, ensuring that they adhere to Lipinski's rule of five and among all the synthesized compounds, only three compounds *i.e.* **4a**, **4b** and **4d** are in range.

Binding and simulation studies: The docking score parameter was used to filter the molecules. The docking scores natural DYRK1A inhibitors (standard), harmine (-6.1 kcal/mol), harmol (-5.8 kcal/mol), staurosporine (-8.7 kcal/mol), acrifoline (-7.4 kcal/mol) and the control {N}2-(3-morpholin-4-yl-propyl)pyrido[3,4-*g*]quinazoline-2,10-diamine bound with protein (-6.0 kcal/mol) are found. The docking score of the natural DYRK1A inhibitor was utilized to develop substituted pyrazolo[4,3-*c*]pyrido[3,2-*e*]pyridazine. Among all the compounds, **4a**, **4b** and **4d** were selected for further dynamic analysis

TABLE-1
LIPNSKI'S RULE OF FIVE AND PHYSIO-CHEMICAL PARAMETERS OF PYRIDO PYRIDAZINE COMPOUNDS

Compd.	log P	m.w.	nON[1]	nOHNH[2]	n Violations	TPSA[3]	nrotb[4]
4a	2.58	289.3	6	0	0	73.57	1
4b	1.34	290.29	7	0	0	86.47	1
4c	2.79	303.32	6	0	0	73.57	2
4d	2.54	334.3	9	0	0	119.4	2
4e	3.21	323.74	6	0	0	73.57	1
4f	3.26	323.74	6	0	0	73.57	1
4g	2.52	305.3	7	1	0	93.8	1

[1]nON: Number of nitrogen; [2]nOHNM: Number of hydroxyl, nitrogen hydrogen; [3]TPSA: Total polar surface area; [4]nrotb: Number of rotatable bonds

(to reassure the designing by analyze parameter) because they showed total polar surface area and logP value.

Compound 4a binding mode and simulation studies: The Autodock Vina binding energy data of compound **4a** with PDB ID: 6Q8K (-10.0 kcal/mol) was compared to the standard PDB ID: 6Q8K (-6.1 to -8.7 kcal/mol) and the complex PDB ID: 6Q8K (-6 kcal/mol). The binding energy difference of compound **4a** with PDB ID: 6Q8K and standard is high. The nitrogen atom of pyrazolo[2,3-c]pyridopyridazine exhibits hydrogen bonding interactions with PHEA:326 and pi-stacking with ILEA:239, along with other binding interactions observed in the compound with 6Q8K (Fig. 2). The docked compound **4a** was further analyzed for stability studies of 10 ns with the molecular dynamics procedure. In Fig. 5, the RMSD representing complex **4a** shows stability for 3 ns and changes continuously for 7 ns. The RMSF represents a few fluctuations of complex **4a**. The radius of gyration represents that complex

4a is stable for 3-4 ns and changes continuously for 7 ns, indicating protein unfolding and not compacting. The hydrogen bond interactions were observed at a distance of 3.5 nm and an angle of fewer than 30°.

Compound 4b binding mode and simulation analysis: The binding energy of compound **4b** with PDBID: 6Q8K (-9.7 kcal/mol) was compared to standard PDBID: 6Q8K (-6.1 to -8.7 kcal/mol) and complex PDB ID: 6Q8K (-6 kcal/mol). Thus, the binding energy difference of PDB ID:6Q8K is high. Carbon hydrogen bond interaction was observed in the methyl group of the pyridine derivative of pyrido-pyridazine nucleus and as hydrogen donor. ALAA: 202 participated in pi-stacking pyridine of pyrido-pyridazine molecule. The hydrogen bond PHEA: 326 with pyrido-pyridazine nucleus of compound **4b** is shown in Fig. 3. In Fig. 5, the MD parameter RMSD represented that complex **4b** is stable for 2 ns and changes continuously for 8 ns, whereas the RMSF represented the partial fluctu-

Fig. 2. Binding interaction of 6Q8K with compound **4a** in (a) 3D and (b) 2D

Fig. 3. Binding interaction of 6Q8K with compound **4b** in (a) 3D and (b) 2D

ation of complex **4b**. Radius gyration of the complex 4b stable was 2 ns and changed continuously for 8 ns, which represents that the unfolding of protein and not compact. The hydrogen bond interaction was observed in between a 3.5 nm distance and an angle less than 30º.

Compound 4d binding mode and simulation analysis: The binding energy of compound **4d** with PDBID 6Q8K (-9.7 kcal/mol) was compared to standard PDBID:6Q8K(-6.1 to -8.7 kcal/mol) and complex PDB: 6Q8K (-6 kcal/mol). Thus, the binding energy difference of PDBID: 6Q8K is high. The hydrogen bond interaction of pyrido-pyridazine nucleus with GLYA:173 and shows the pi-alkyl interaction of pyridopyridazine nucleus with ILEA:239 and VALA:193, but no pi-amide stacking was observed in compound **4d** (Fig. 4). The MD parameter RMSD represented that complex **4d** was stable for 4.5 ns and changed continuously for 5.5 ns. The RMSF represented a fluctuation of 0.5 ns of complex **4d** (Fig. 5). Radius gyration represented that complex **4d** was for stable 5 ns and changed continuously for 5 ns, which represent that protein equally fold and unfold and has less compact. The hydrogen bond interaction was observed between a 3.5 nm distance and an angle of fewer than 30º.

Binding free energy: The binding free energy of the complex was determined from the molecular dynamic trajectories by the MMPBSA method. Using eqn. 1, the free energy was calculated in order to determine the compound receptor system.

$$\Delta G = G_{RC} - (G_R + G_C) \qquad (1)$$

The free energy for each individual is given eqn. 2, where Z represents the receptor-compound complex, E_{MM} molecular mechanics potential energy in a vacuum, and G_S was the free energy of solvation; temperature and entropy representing the TS entropic contribution of free energy in the vacuum.

$$G_Z = E_{MM} + G_{SOL} - TS_{MM} \qquad (2)$$

The sum of polar and non-polar energy is the solvation energy as according to eqn. 3:

$$G_{solv} = G_{polar} + G_{non-polar} \qquad (3)$$

where E_{MM} have bonded and non-bonded interaction energy which is due to the electrostatic (E_{MM}) and van der Waals (E_{VDW}) interaction

$$E_{MM} = E_{non-bonded} + E_{bonded} + (E_{VDW} + E_{elec}) \qquad (4)$$

The entropy data cannot be provided since it was not calculated by the gmxMMPBSA tool. The MMPBSA binding free energy of the complex is summarized in Table-2. The total energy of compounds **4a**, **4b** and **4d** in comparison with standard and harmine is not favourable. The total free energy of standard and harmine is 17.3, 17.83, respectively while for **4a**, **4b**, **4d** 44.82, 20.73, 26.2 respectively. A similar observation in van der wall and electrostatic energy. The solvent accessible area observation reveals similarity thus, hydrophobic interaction is observed between the compound and protein (Fig. 6).
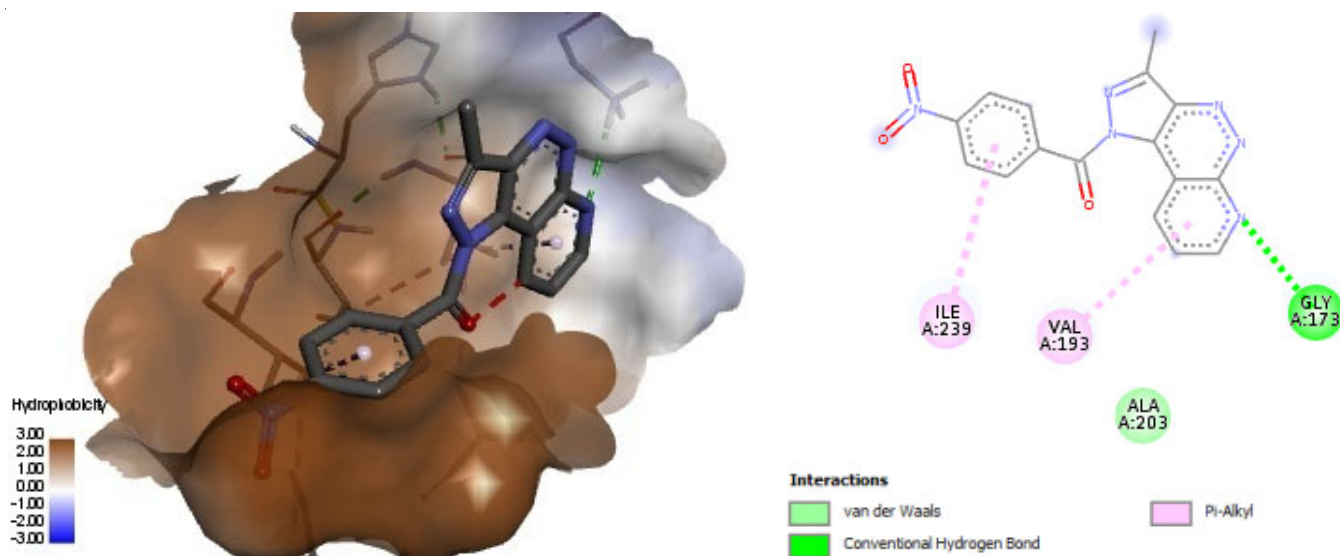
Fig. 4. Binding interaction of 6Q8K with compound **4d** in (a) 3D and (B) 2D

TABLE-2
COMPLEX – RECEPTOR – LIGAND BINDING FREE ENERGY (MMPBSA)

Energy component	Standard	Harmine	4a	4b	4d
ΔVDWAALS	-18.32	-19.78	-21.68	-27.16	-31.28
ΔEEL	-13.33	-29.89	-43.08	-32.81	-38.7
ΔEPB	33.72	53.99	95.63	63.02	75.56
ΔENPOLAR (SASA)	-14.97	-17.06	-19.57	-19.76	-22.93
ΔEDISPER	30.2	30.56	33.51	37.44	43.55
ΔGGAS	-31.65	-49.67	-64.76	-59.97	-69.98
ΔGSOLV	48.95	67.5	109.58	80.7	96.18
ΔTOTAL	17.3	17.83	44.82	20.73	26.2
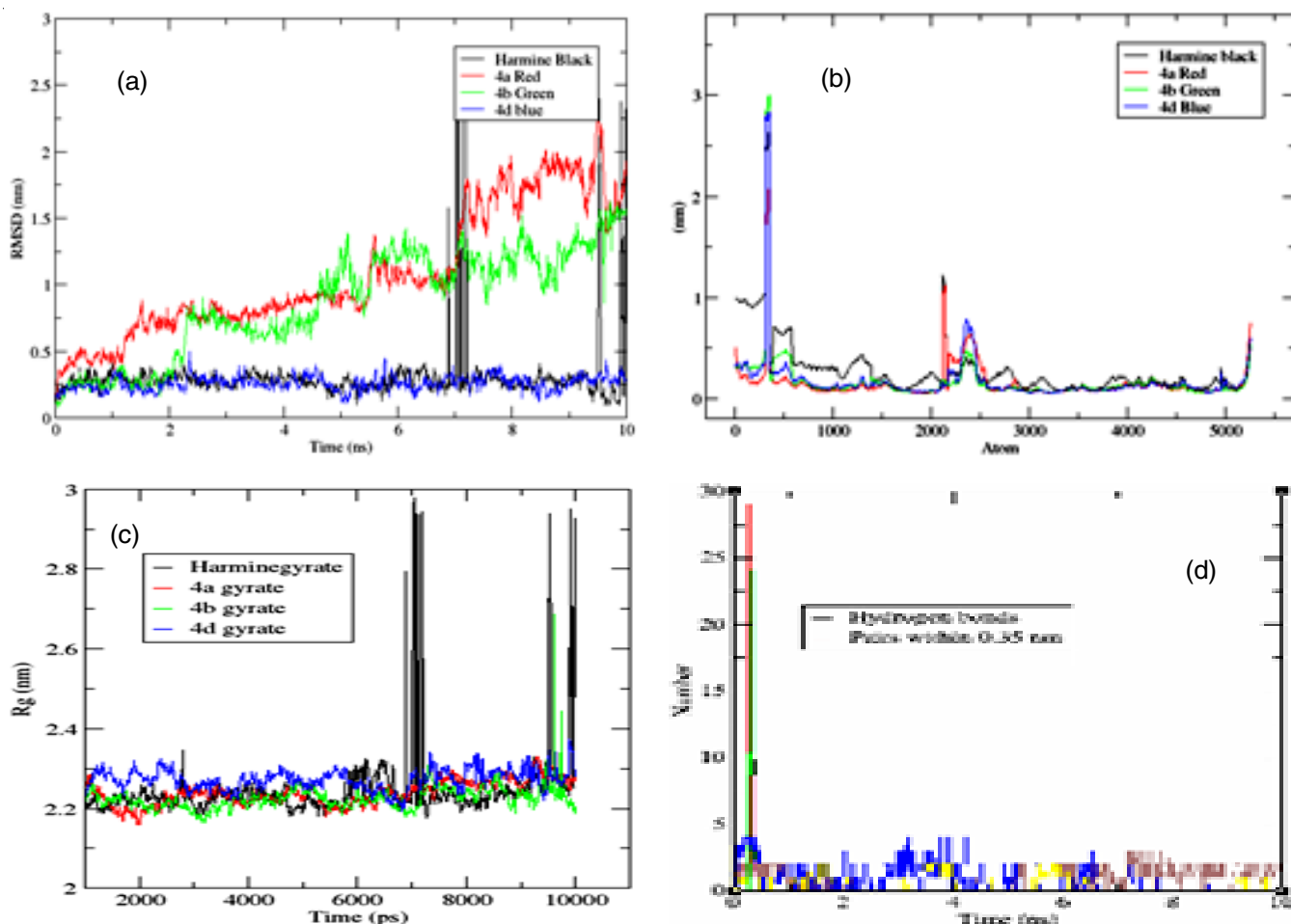
Fig. 5. Molecular dynamics (a) molecular dynamic simulation time *versus* RMSD, (b) molecular dynamic simulation atom *versus* distance, (c) radius of gyration, (d) hydrogen bond interaction
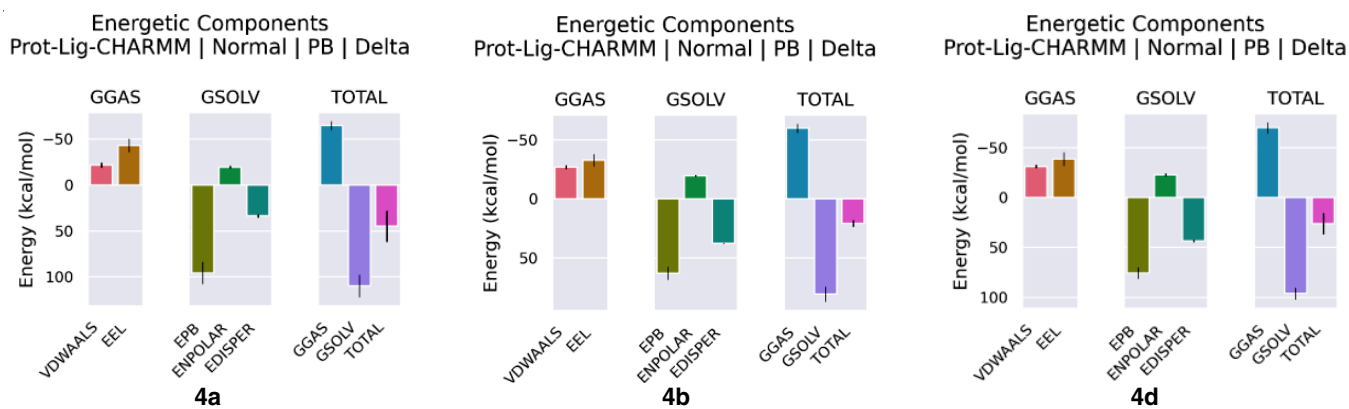
Fig. 6. Binding free energy of compounds **4a**, **4b** and **4d** with protein

Biological activity: The cancer metastasis and growth were supported by bacteria and it synergize by acidic pH. Thus, the antibacterial activity of compounds has to be required. The antibacterial screening of both Gram strains (Gram positive *Staphylococcus aureus* and Gram negative *Escherichia coli*) against the compounds were encouraging and synergize it response (Table-3). Specifically, compound **4a** exhibited 14.56% inhibition against kidney cancer using the UO-31 cell lines.

Compound **4b** demonstrated 12% inhibition against Neuroblastoma using the SNB-75 cell line. It also displayed 39% inhibition against renal cancer using the A-498 cell line and 32% inhibition against kidney cancer using the UO-31 cell line. Compound **4d** showed 8% inhibition against Neuroblastoma using the SNB-75 cell line, 4% inhibition against ovarian cancer using the OVCAR-8 cell line and 14% inhibition against kidney cancer using the UO-31 cell line.

TABLE-3		
ANTIMICROBIAL SCREENING OF COMPOUNDS		
Compound	50 μg	75 μg
4a	56	68
4b	64	72
4c	68	76
4d	60	72
4e	60	84
4f	56	84
4g	64	84

Conclusion

This study began by designing polycyclic compounds with specific features, including the presence of two cyclic rings and three nitrogen atoms, based on some natural DYRK1A inhibitor. The newly designed derivatives containing pyrazolo[2,3-*c*]-pyrido-pyridazine scaffold were synthesized and characterized by using NMR, mass and IR spectroscopy. These compounds were subsequently screened for their pharmacokinetic properties and expected for DYRK1A activity using SBDD method. The docking scores of all the synthesized compounds ranged from -6.5 to -10 kcal/mol, indicating favourable binding to the target. Notably, three compounds (**4a**, **4b** and **4d**) displayed higher docking scores ranging from -9.5 to -10 kcal/mol. Moreover, these compounds adhered to the Lipinski's rule, which is indicative of their potential as drugs. Further analysis revealed that these compounds exhibited stability, compactness and effective hydrogen bonding for a duration of 3 ns. Based on the computational data and the promising results of compounds **4a**, **4b** and **4d** were selected for further *in vitro* anticancer screening. Cancer metastasis to be synergies with bacterial infection thus, need antibacterial effects. Compounds **4a-g** have antibacterial activity 68-88% inhibition.

CONFLICT OF INTEREST

The authors declare that there is no conflict of interests regarding the publication of this article.

REFERENCES

1. K.D. Seely, A.D. Morgan, L.D. Hagenstein, G.M. Florey and J.M. Small, *Cancers*, **14**, 1019 (2022);
https://doi.org/10.3390/cancers14041019

2. L. Litovchick, L.A. Florens, S.K. Swanson, M.P. Washburn and J.A. DeCaprio, *Genes Dev.*, **25**, 801 (2011);
https://doi.org/10.1101/gad.2034211

3. A. Kamb, S. Wee and C. Lengauer, *Nat. Rev. Drug Discov.*, **6**, 115 (2007);
https://doi.org/10.1038/nrd2155

4. P. Fernández-Martínez, C. Zahonero and P. Sánchez-Gómez, *Mol. Cell. Oncol.*, **2**, e970048 (2015);
https://doi.org/10.4161/23723548.2014.970048

5. A.R.I. Altaba, *Sci. Signal.*, **4**, 9 (2011);
https://doi.org/10.1126/scisignal.200254

6. J. Mao, P. Maye, P. Kogerman, F.J. Tejedor, R. Toftgard, W. Xie, G. Wu and D. Wu, *J. Biol. Chem.*, **277**, 35156 (2002);
https://doi.org/10.1074/jbc.M206743200

7. C.C. Wu and S.B. Bratton, *Mol. Cell. Oncol.*, **4**, e1281865 (2017);
https://doi.org/10.1080/23723556.2017.1281865

8. A. Laguna, S. Aranda, M.J. Barallobre, R. Barhoum, E. Fernández, V. Fotaki, J.M. Delabar, S. de la Luna, P. de la Villa and M.L. Arbonés, *Dev. Cell*, **15**, 841 (2008);
https://doi.org/10.1016/j.devcel.2008.10.014

9. X. Guo, J.G. Williams, T.T. Schug and X. Li, *J. Biol. Chem.*, **285**, 13223 (2010);
https://doi.org/10.1074/jbc.M110.102574

10. A. Ionescu, F. Dufrasne, M. Gelbcke, I. Jabin, R. Kiss and D. Lamoral-Theys, *Mini-Rev. Med. Chem.*, **12**, 1315 (2012);
https://doi.org/10.2174/13895575112091315

11. N. Pozo, C. Zahonero, P. Fernández, J.M. Liñares, A. Ayuso, M. Hagiwara, A. Pérez, J.R. Ricoy, A. Hernández-Laín, J.M. Sepúlveda and P. Sánchez-Gómez, *J. Clin. Invest.*, **123**, 2475 (2013);
https://doi.org/10.1172/JCI63623

12. D.B. Jarhad, K.K. Mashelkar, H.R. Kim, M. Noh and L.S. Jeong, *J. Med. Chem.*, **61**, 9791 (2018);
https://doi.org/10.1021/acs.jmedchem.8b00185

13. M.A. Ibrahim, A.H. Elmenoufy, M. Elagawany, M.M. Ghoneim and A. Moawad, *J. Biosci. Med.*, **3**, 59 (2015);
https://doi.org/10.4236/jbm.2015.310008

14. R.K. Tonk, S. Bawa, G. Chawla, G.S. Deora, S. Kumar, V. Rathore, N. Mulakayala, A. Rajaram, A.M. Kalle and O. Afzal *Eur. J. Med. Chem.*, **57**, 176 (2012);
https://doi.org/10.1016/j.ejmech.2012.08.045

15. A. Daina, O. Michielin and V. Zoete, *Sci. Rep.*, **7**, 42717 (2017);
https://doi.org/10.1038/srep42717

16. G.M. Morris, H. Ruth, W. Lindstrom, M.F. Sanner, R.K. Belew, D.S. Goodsell and A.J. Olson, *J. Comput. Chem.*, **30**, 2785 (2009);
https://doi.org/10.1002/jcc.21256

17. G.M. Morris, D.S. Goodsell, R.S. Halliday, R. Huey, W.E. Hart, R.K. Belew and A.J. Olson, *J. Comput. Chem.*, **19**, 1639 (1998);
https://doi.org/10.1002/(SICI)1096-987X(19981115)19:14<1639::AID-JCC10>3.0.CO;2-B

18. BIOVIA, Dassault Systèmes BIOVIA, Discovery Studio Modeling Environment, Release 2017, Dassault Systèmes (2017).

19. H. Tazarki, W. Zeinyeh, Y.J. Esvan, S. Knapp, D. Chatterjee, M. Schröder, A.C. Joerger, J. Khiari, B. Josselin, B. Baratte, S. Bach, S. Ruchaud, F. Anizon, F. Giraud and P. Moreau, *Eur. J. Med. Chem.*, **166**, 304 (2019);
https://doi.org/10.1016/j.ejmech.2019.01.052

20. S. Zhu, *J. Chem. Inf. Model.*, **59**, 4239 (2019);
https://doi.org/10.1021/acs.jcim.9b00552

21. P.A. Kollman, I. Massova, C. Reyes, B. Kuhn, S. Huo, L. Chong, M. Lee, T. Lee, Y. Duan, W. Wang, O. Donini, P. Cieplak, J. Srinivasan, D.A. Case and T.E. Cheatham, *Acc. Chem. Res.*, **33**, 889 (2000);
https://doi.org/10.1021/ar000033j